Provided for non-commercial research and education use.
Not for reproduction, distribution or commercial use.

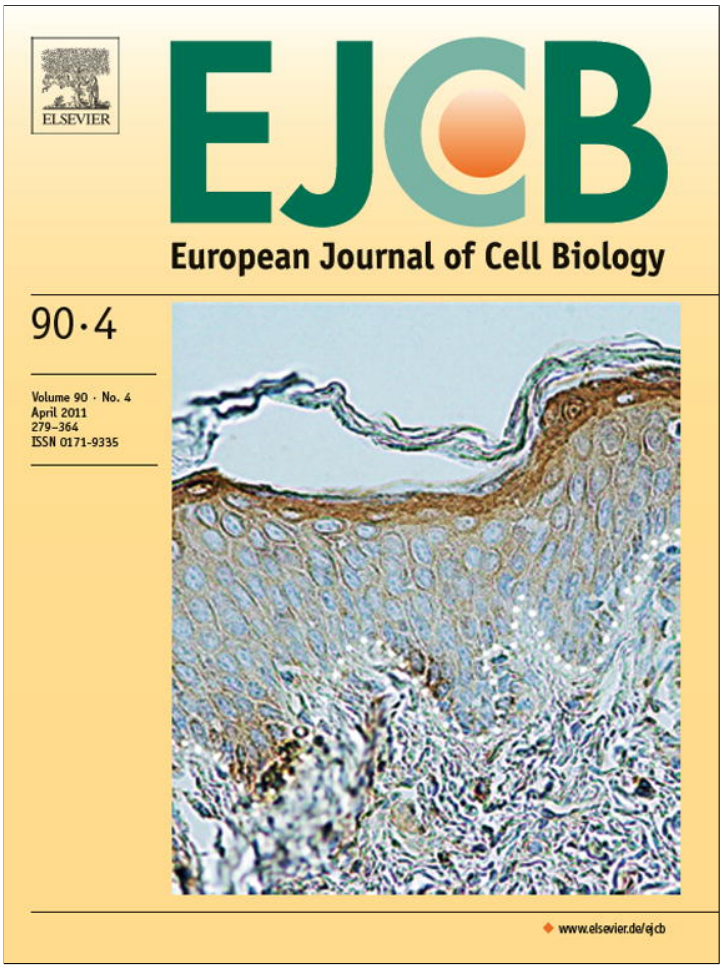

This article appeared in a journal published by Elsevier. The attached copy is furnished to the author for internal non-commercial research and education use, including for instruction at the authors institution and sharing with colleagues.

Other uses, including reproduction and distribution, or selling or licensing copies, or posting to personal, institutional or third party websites are prohibited.

In most cases authors are permitted to post their version of the article (e.g. in Word or Tex form) to their personal website or institutional repository. Authors requiring further information regarding Elsevier's archiving and manuscript policies are encouraged to visit:

http://www.elsevier.com/copyright

Author's personal copy

European Journal of Cell Biology 90 (2011) 342–355

Contents lists available at ScienceDirect

European Journal of Cell Biology

journal homepage: www.elsevier.de/ejcb

The Ras related GTPase Miro is not required for mitochondrial transport in *Dictyostelium discoideum*

Georgia Vlahou[a], Marek Eliáš[b,c], Jürgen-Christoph von Kleist-Retzow[d,e], Rudolf J. Wiesner[e,f,g], Francisco Rivero[a,h,*]

[a] Zentrum für Biochemie, Medizinische Fakultät, Universität zu Köln, Joseph-Stelzmann-Strasse 52, 50931 Köln, Germany
[b] Charles University in Prague, Faculty of Science, Departments of Botany and Parasitology, Benatska 2, 128 01 Prague 2, Czech Republic
[c] University of Ostrava, Faculty of Science, Department of Biology and Ecology, Chitussiho 10, 710 00 Slezska Ostrava, Czech Republic
[d] Klinik und Poliklinik für Kinderheilkunde, Medizinische Fakultät, Universität zu Köln, Kerpener Str. 62, 50937 Köln, Germany
[e] Center for Molecular Medicine Cologne (CMMC), Universität zu Köln, Joseph-Stelzmann-Str. 52, 50931 Köln, Germany
[f] Institute of Vegetative Physiology, Medizinische Fakultät, Universität zu Köln, Robert-Koch-Str. 39, 50931 Köln, Germany
[g] CECAD (Cologne Excellence Cluster on Cellular Stress Responses in Aging-Associated Diseases), Institute for Genetics, Universität zu Köln, Zülpicher Str. 47a, 50674 Köln, Germany
[h] Centre for Biomedical Research, The Hull York Medical School and Department of Biological Sciences, University of Hull, Cottingham Road, Hull HU6 7RX, UK

ARTICLE INFO

Article history:
Received 28 April 2010
Received in revised form 22 October 2010
Accepted 26 October 2010

Keywords:
Miro
Mitochondrial transport
Small GTPase
Dictyostelium

ABSTRACT

Ras-related GTPases of the Miro family have been implicated in mitochondrial homeostasis and microtubule-dependent transport. They consist of two GTP-binding domains separated by calcium-binding motifs and of a C-terminal transmembrane domain that targets the protein to the outer mitochondrial membrane. We disrupted the single Miro-encoding gene in *Dictyostelium discoideum* and observed a substantial growth defect that we attribute to a decreased mitochondrial mass and cellular ATP content. However, mutant cells even showed an increased rate of oxygen consumption, while glucose consumption, mitochondrial transmembrane potential and production of reactive oxygen species were unaltered. Processes characteristic of the multicellular stage of the *D. discoideum* life cycle were also unaltered. Although mitochondria occasionally use microtubules for transport in *D. discoideum*, their size and distribution were not visibly affected. We found Miro in all branches of the eukaryotic tree with the exception of a few protist lineages (mainly those lacking typical mitochondria). Trypanosomatids and ciliates possess structurally unique homologs lacking the N-terminal or the C-terminal GTPase domain, respectively. We propose that in *D. discoideum*, as in yeasts and plants, Miro plays roles in mitochondrial homeostasis, but the ability to build a complex that regulates its association to kinesin for microtubule-dependent transport probably arose in metazoans.

© 2010 Elsevier GmbH. All rights reserved.

Introduction

Mitochondria are key players in many fundamental biological processes and undergo constant changes in shape and distribution. They are the main organelle for aerobic energy production and supply a variety of intermediates that are required for cellular metabolism. Furthermore, mitochondria are involved in a range of other vital cellular processes including Ca^{2+} homeostasis, but also formation of reactive oxygen species (ROS) and oxidative stress, and as integral parts of signaling cascades they participate in the regulation and execution of programmed cell death, cellular differentiation and the control of the cell cycle and cell growth (McBride et al., 2006). Consequently, an impaired mitochondrial function can lead to a multitude of diseases, most importantly neurodegenerative disorders, as neurons rely on a constant supply of ATP but also efficient mitochondrial trafficking for energy supply especially at synaptic endings (DiMauro, 2004).

Miro GTPases have been identified recently as key components in mitochondrial dynamics (Liu and Hajnoczky, 2009; Reis et al., 2009). They belong to the Ras superfamily of small GTPases and consist of two GTPase domains separated by a linker region containing two EF hand motifs, which were shown recently to bind Ca^{2+} (MacAskill et al., 2009a). The first GTPase domain has sequence similarity to proteins of the Ras superfamily, whereas the second GTPase domain is only distantly related to those (Fransson et al., 2003). Notably, Miro proteins are anchored to the outer mitochondrial membrane by virtue of a short transmembrane region at the C-terminus whereas the remaining domains are exposed to the cytosol (Frederick et al., 2004; Fransson et al., 2006). So far, Miro proteins have been characterized in metazoa, yeasts, and plants

* Corresponding author at: Centre for Biomedical Research, The Hull York Medical School, University of Hull, Wolfson Building, Room 506, Hull HU6 7RX, UK. Tel.: +44 1482 466433; fax: +44 1482 465008.
E-mail address: Francisco.rivero@hyms.ac.uk (F. Rivero).

0171-9335/$ – see front matter © 2010 Elsevier GmbH. All rights reserved.
doi:10.1016/j.ejcb.2010.10.012

Author's personal copy

(for a recent review see Reis et al., 2009), but their phylogenetic distribution and function in other eukaryotic lineages remains to be explored.

In early reports Miro proteins were implicated in the regulation of mitochondrial morphology and possibly also apoptosis based on studies of overexpression of the two mammalian isoforms (Fransson et al., 2003). *S. cerevisiae* cells lacking the Miro homolog Gem1p showed altered mitochondrial distribution described as collapsed, globular or grape-like (Frederick et al., 2004). Miro was shown not to be required for mitochondrial fission and fusion events, although it influences mitochondrial inheritance in yeast (Frederick et al., 2008). In *A. thaliana* three genes encoding putative Miro-related GTPases have been described. The EMB2473/MIRO1 mutant exhibits abnormally enlarged or tube-like mitochondrial morphology, resulting in the disruption of continuous streaming of mitochondria in the growing pollen tube. Furthermore it was shown that MIRO1 plays a decisive role in the process of embryogenesis, whereas mutations in the MIRO2 gene do not have any obvious influence on plant development (Yamaoka and Leaver, 2008). In *D. melanogaster* loss of dMiro causes a derangement of the axonal mitochondrial transport, resulting in impaired larval locomotion and disrupted subcellular distribution of mitochondria in neurons and muscles (Guo et al., 2005). More recent work based on overexpression or loss of dMiro in larval axons suggest that this protein is required for both anterograde and retrograde mitochondrial transport through modulation of the processivity of kinesin and dynein (Russo et al., 2009).

Axonal mitochondrial transport requires Milton, an adaptor protein that binds dMiro and recruits the heavy chain of kinesin-1 (KHC) to mitochondria independently of the kinesin light chain (KLC) (Glater et al., 2006). An interaction of mammalian Miro with Milton-related kinesin-binding proteins GRIF-1 and OIP106 has been reported, suggesting that in metazoa Miro GTPases form a link between the mitochondria and the microtubule trafficking apparatus (Fransson et al., 2006; MacAskill et al., 2009b). Additional studies provide evidence that Miro functions as a calcium sensor that regulates mitochondrial motility in response to intracellular calcium fluctuations (Saotome et al., 2008; MacAskill et al., 2009b; Wang and Schwarz, 2009). Although contradictory models have been put forward to explain the functioning of the Miro/Milton/KHC complex, it is accepted that increased intracellular calcium levels are sensed by the EF hands of Miro, and the associated conformational change alters the complex, resulting in reduced mitochondrial motility (Liu and Hajnoczky, 2009; Reis et al., 2009). Further interaction partners of Miro have been reported recently, like the PTEN-induced kinase Pink-1 and the hypoxia up-regulated mitochondrial movement regulator HUMMR that play roles in mitochondrial trafficking, but their mechanisms of Miro modulation have not been established yet (Li et al., 2009; Weihofen et al., 2009).

In this study we investigate the role of Miro taking advantage of *Dictyostelium discoideum* as a model organism. *D. discoideum* is suitable to analyze a broad repertoire of cellular processes, including structural and regulatory aspects of the cytoskeleton, signal transduction as well as cell-type differentiation and developmental processes. In addition, *D. discoideum* is susceptible to a variety of biochemical, molecular genetics and cell biology approaches. Mitochondrial homeostasis, and in particular mitochondrial dynamics, has been poorly investigated in *D. discoideum*. Here the single gene encoding the *D. discoideum* ortholog, *gemA*, was knocked out and mutants were analyzed for a variety of different processes known to be required for or affected by mitochondrial functioning. We show that although in *D. discoideum* mitochondria are occasionally connected to the microtubule network, ablation of Miro does not result in altered morphology or distribution of these organelles, but rather affects mitochondrial metabolism. This prompted us to define the phylogenetic distribution of the Miro family in eukaryotes and describe its evolution and diversity of domain architectures. We propose that in *D. discoideum*, as opposed to metazoa, Miro plays ancestral roles unrelated to mitochondrial transport.

Materials and methods

Growth and development of D. discoideum

D. discoideum AX2 cells and transformants were grown either at 21 °C in liquid nutrient medium with shaking at 160 rpm or on SM agar plates with *Klebsiella aerogenes* (Newell et al., 1969). For development, cells were grown to a density of 2×10^6 cells/ml and washed in Soerensen buffer (2 mM Na_2HPO_4, 14.6 mM KH_2PO_4 pH 6) and 0.5×10^8 cells were deposited on phosphate agar plates and allowed to develop at 21 °C (Newell et al., 1969). For development under submerged conditions 2×10^5 cells/cm^2 well were plated on plastic dishes in Soerensen buffer and starved at 21 °C.

Protein expression and purification and antibody generation

A DNA fragment encoding the first GTPase domain (176 aa) of Miro was obtained by reverse transcriptase PCR using M-MLV RNase H (Promega, Madison, WI, United States) and primers Miro-fwd/B GGA TCC ATG AAA AAT AAC ATA AAG GTT ATT TTA ATT GG and Miro-rev/R GAA TTC TTA TGC ACG TTC ACA TCC TTC AGT C. The PCR fragment was cloned into pGEM-Teasy (Promega, Madison, WI, USA), verified by DNA sequencing, excised with BamHI and PstI and subcloned into the pQE30 bacterial expression vector (Qiagen GmbH, Hilden, Germany). The 21 kDa His-tagged protein was expressed using standard procedures. Bacterial lysate was resolved on a preparative SDS PAGE and the band of interest was excised from the gel and electroeluted. The protein was used for immunization of 6 Balb/c mice with 10 μg of purified protein. The mice were boosted once per week with 10 μg of protein for four weeks and then sacrificed for isolation of knee lymph node lymphocytes, which were fused to the myeloma cell lines Ag8 and PAI (Lingnau et al., 1996). Hybridomas were screened for their ability to recognize the antigen on ELISA plates and Western blots. Monoclonal antibodies K72-642-1 and K72-642-2 were selected for further studies.

Plasmids and strains

A genomic DNA fragment comprising full-length Miro was amplified using PCR on *D. discoideum* DNA with Miro-fwd/B GGA TCC ATG AAA AAT AAC ATA AAG GTT ATT TTA ATT GG and Miro-rev/B GGA TCC TTA TTT TTT AGC TAA ATA TTT ACT TAA AAG primers. The PCR product was cloned in pGEMTeasy (Promega, Madison, WI, USA) and verified by DNA sequencing. The full length clone was used as a template for amplification of the transmembrane region with MiroTM-fwd-GGA TCC AAT TCC ATT TAT CAC GAG ATG and Miro-rev/B. A Miro ΔTM fragment was cut out from the full length clone using BamHI and an internal BglII restriction site placed between the second GTPase domain and the transmembrane region. The fragments were subcloned into the BamHI site of a pDEX-GFP derivative (Westphal et al., 1997) to generate vectors that allowed expression of the red-shifted S65T mutant form of *Aequorea victoria* GFP fused to the N terminus of the proteins in *D. discoideum* under the control of the actin-15 promoter. Plasmid DNA was electroporated into *D. discoideum* cells. Transformants were grown on selective medium containing 20 μg/ml G418 and clonal populations were obtained by serial dilution in microtiter plates. GFP-expressing transformants were confirmed by visual inspection under a fluorescence microscope.

Author's personal copy

Disruption of the *gemA* gene is described in Figure S1. Briefly, a construct was generated in which 1.8 kb of the gene was replaced by a 1.3 kb bsr resistance cassette (Adachi et al., 1994). The knock-out vector was linearized and electroporated into *Dictyostelium* cells. Transformants were grown on selective medium containing 3 μg/ml blasticidin S. Single colonies were obtained by spreader dilution of the whole pool of transformants onto SM agar plates overlaid with *Klebsiella aerogenes*. Disruption of the *gemA* gene was verified using PCR, Southern blot and Western blot as described in Figure S1.

Antibodies and staining dyes

Actin was detected using mAb Act 1-7 (Simpson et al., 1984), mitochondria using a mAb against porin (Troll et al., 1992), tubulin using mAb YL1/2 (Kilmartin et al., 1982) and mAb WA3 (gift from Dr. Ursula Euteneuer), contact site A using mAb 33-294-17 (Bertholdt et al., 1985), GFP using mAb K3-184-2 (Noegel et al., 1999) and DdKif5 using a specific antiserum (Iwai et al., 2004). The appropriate Cy3 or Alexa Fluor-labeled anti-mouse immunoglobulins (Molecular Probes) were used as secondary antibodies. Nuclei were stained with DAPI (4′,6′-diamidino-2-phenylindole; Sigma–Aldrich, St. Louis, MO). MitoTracker Red and MitoTracker Green (Molecular Probes, Invitrogen, Karlsruhe, Germany) were used to visualize mitochondria in fixed and living cells following the recommendations of the manufacturer.

Conventional and fluorescence microscopy

Cells were fixed in cold methanol (−20 °C) or at room temperature with picric acid/paraformaldehyde (15% of a saturated aqueous solution of picric acid, 2% paraformaldehyde [v/v], pH 6.0), followed by 70% ethanol. To investigate the effect of cytoskeleton disrupting drugs cells were allowed to attach to coverslips and were incubated for 3 h with 30 μg/ml nocodazole or 30 min with 20 μM cytochalasin A or 2 μM latrunculin B (Sigma, St. Louis, MO) prior to fixation. Confocal images were taken with an inverted Leica TCS-SP confocal laser-scanning microscope with a 100× HCX PL APO NA 1.40 oil immersion objective. For excitation, the 488 nm argon-ion laser line and the 543 nm HeNe laser line were used. Images were processed using the accompanying software.

Development and phototaxis were documented with a Leica MZFLIII stereomicroscope equipped with a Hitachi HV-C20A video camera. To assay chemotaxis aggregation competent cells were stimulated with a glass capillary micropipette (Femtotip, Eppendorf, Hamburg, Germany) filled with 0.1 mM cAMP (Abo et al., 1991). Time-lapse image series were captured with a charge coupled device (CCD) camera and stored on a computer hard drive at 30 s intervals. The DIAS software (Soltech, Oakdale, IA, USA) was used to trace individual cells along the image series and determine cell motility parameters (Adachi et al., 1994).

To assay cytokinesis axenically growing cells were fixed with methanol and nuclei stained with DAPI. The number of nuclei per cell was scored using a conventional inverted fluorescence microscope (1X70, Olympus) equipped with a 40× objective and a CVM10 (CCD) camera (Progressive Scan, Japan). Cell diameters of fixed cells were measured from images using image J (Rivero et al., 1996). The same setup with a 100× objective was used to capture the time lapse series of cells stained with MitoTracker Green.

Cell biology methods

Phagocytosis was assayed using TRITC-labeled yeast particles and fluid-phase endocytosis and exocytosis was assayed using FITC-dextrane as described (Rivero and Maniak, 2006). To assay phototaxis vegetative cells were washed twice in water before placing 10^6 cells on the center of 1% water agar plates. The plates were incubated in a dark box with a 3 mm wide vertical slit in constant light for 48 h at 21 °C. Slime trails were blotted onto nitrocellulose filters, stained with 1% amido black in 25% isopropanol and 10% acetic acid for 10 min, distained in 25% isopropanol and 10% acetic acid, and washed with water and air dried.

Biochemical methods

The mitochondrial transmembrane potential was measured with a Mitochondria Staining Kit (Sigma–Aldrich GmbH, Munich, Germany). Exponential growth phase cells were washed twice and were allowed to recover in low fluorescence nutrient medium (FORMEDIUM Ltd, Hunstanton, United Kingdom) for 30 min and stained in the same medium containing 200 nM JC-1 (5,5′,6,6′-tetrachloro-1,1′,3,3′-tetraethylbenzimidazole carbocyanide iodide; Sigma–Aldrich, Munich, Germany) for 30 min at 21 °C in a dark room. After washing, 1×10^4 cells were resuspended in fresh Soerensen buffer and fluorescence was analyzed with a Fluoroskan fluorimeter (BD Bioscience, Heidelberg, Germany) at excitation 488 nm/emission 590 and 520 nm. To measure ROS cells were processed in the same way as for JC-1 staining except that cells were incubated in 100 M DCFH-DA (dichlorofluorescein diacetate; Sigma–Aldrich, Munich, Germany) for 45 min. The deacetylated DCFH is preferentially oxidized by H_2O_2 and superoxide to the fluorescent dichlorofluorescein, which was analyzed at 525 nm with excitation at 485 nm.

The ATP content was determined using a luciferase-based kit (ENLITEN, Promega, Madison, WI, USA) in cells grown axenically. ATP concentrations were determined from a standard curve following the instructions of the manufacturer.

MitoTracker Green fluorescence was used to estimate mitochondrial mass (Pendergrass et al., 2004). Axenically growing cells were harvested, washed once in Lo-Flo HL-5 medium, allowed to recover in Lo-Flo medium for 2 h and incubated with 200 nM MitoTracker Green FM (Molecular Probes, Invitrogen, Karlsruhe, Germany) for 1 h in the dark. After washing the cells were resuspended in Lo-Flo HL-5 and fluorescence was measured in a fluorimeter (Photon Technology Intl., Seefeld, Germany) at excitation 490 nm/emission 516 nm.

Oxygen consumption was measured polarographically using a Clark-type oxygen electrode (Hansatech Instruments Limited, King's Lynn, UK). Cells were washed, resuspended in PDF buffer (20 mM KCl, 5 mM Mg_2Cl, 20 mM KPO_4 pH 6.4) and placed in a respiration chamber at room temperature. Oxygen consumption was measured for the duration of 5 min after equilibration of the electrode. For the determination of glucose consumption axenically growing cells were harvested over three days, centrifuged and the supernatant stored at −20 °C. The glucose content of the supernatant was measured using a radiometer ABL System 615 (Radiometer Medical Inc., Copenhagen, Denmark).

Miscellaneous methods

DNA was isolated, transferred to nylon membranes and hybridized as described by Rivero et al. (1999). For immunoprecipitation cells were lysed with 50 mM Tris–HCl pH 8.0, 150 mM NaCl, 1% Triton X-100 and protease inhibitors for 30 min. After clearing by centrifugation at 10,000 × *g* at 4 °C, immunoprecipitation was performed using a μMACS epitope tag protein isolation kit (Miltenyi Biotec, Bergisch Gladbach, Germany). For Western blot proteins were resolved on 10% or 12% polyacrylamide/0.1% SDS gels (Ausubel et al., 2001), transferred to nitrocellulose membranes and probed with the indicated primary antibodies followed by incubation with the appropriate peroxidase-coupled IgG (Dianova, Hamburg, Germany) and enhanced chemiluminescence reaction

Author's personal copy

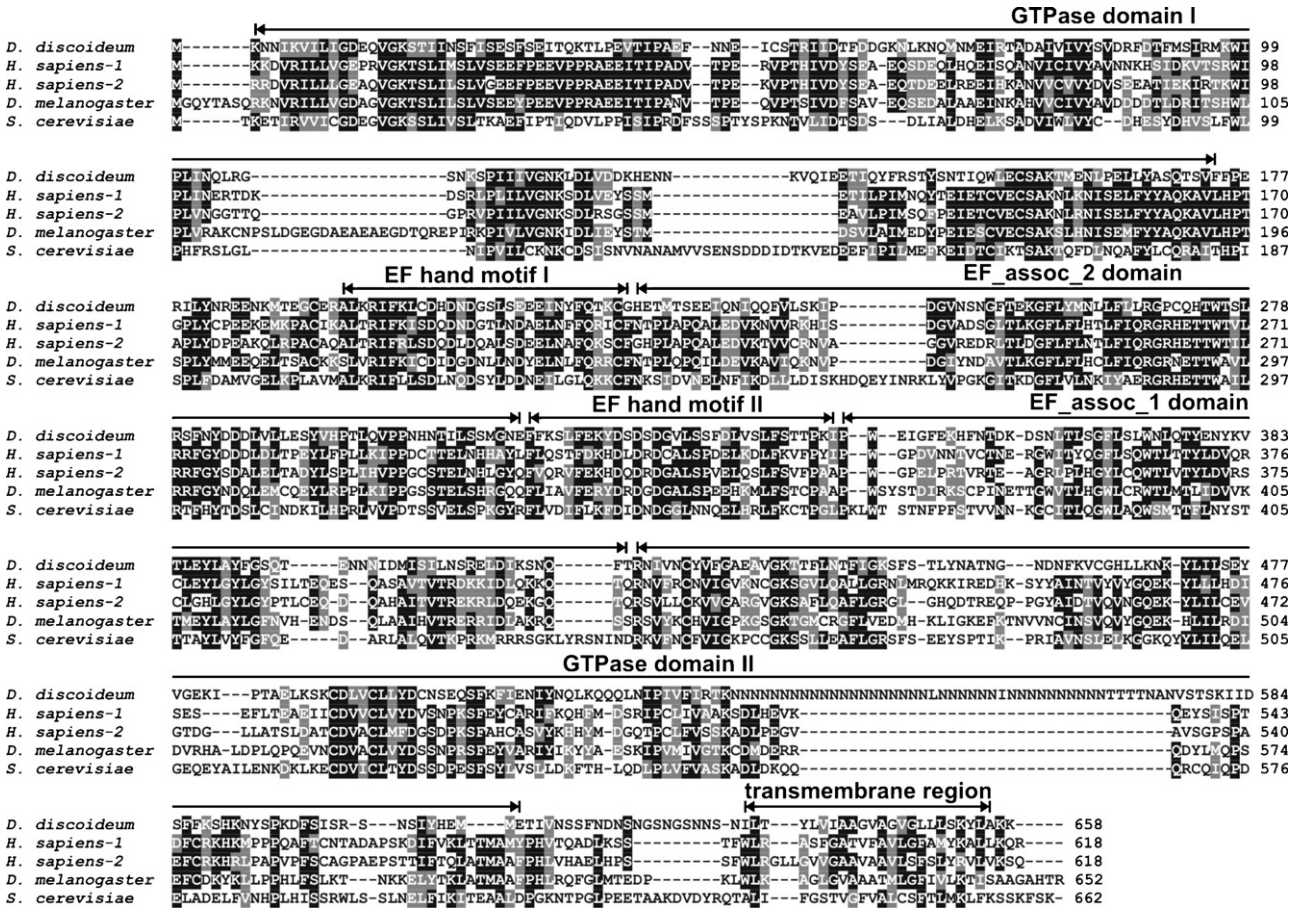

Fig. 1. Sequence analysis of *D. discoideum* Miro. Alignment of the predicted amino acid sequences of *D. discoideum*, *H. sapiens* (Miro-1 and 2), *D. melanogaster* (dMiro), and *S. cerevisiae* (Gem1p) Miro GTPases. Black boxes indicate identical amino acid residues, gray boxes indicate conserved amino acid substitutions. The extension of each domain of Miro is indicated. The alignment is a reduced version of a more extensive alignment available as Figure S5.

(Amersham-Pharmacia, GE Healthcare, Buckinghamshire, United Kingdom).

Sequence searches and phylogenetic analyses

Miro protein sequences were identified using *blastp* and *tblastn* searches against genome, EST and predicted protein sequences available in the National Center for Biotechnology information (NCBI) database (http://www.ncbi.nlm.nih.gov/) and databases maintained by various genome centers. See Table S2 for the sources of individual sequences. A multiple alignment was built with PROMALS (http://prodata.swmed.edu/promals/promals.php) (Pei and Grishin, 2007) and adjusted manually using GeneDoc (http://www.nrbsc.org/gfx/genedoc/). For phylogenetic analyses ambiguously aligned positions were removed and the remaining 442 aligned positions were subjected to a maximum likelihood (ML) tree inference using PhyML 3.0 (Guindon and Gascuel, 2003) run by the Phylogeny.fr server (http://www.phylogeny.fr/version2_cgi/one_task.cgi?task_type=phyml). The tree search was performed using the JTT+Γ4+I substitution model with parameters (gamma distribution parameter and proportion of invariable sites) estimated from the data. 100 bootstrap trees were inferred using the same setting. To assess the robustness of the results obtained with PhyML, an alternative ML procedure as implemented in RAxML 7.0.4 was employed. This analysis was done using the CIPRES (Cyberinfrastructure for Phylogenetic Research) Portal (http://www.phylo.org/sub_sections/portal/) and the rapid bootstrapping algorithm followed by a full ML tree search (as described in Stamatakis et al., 2008). The resulting tree was highly congruent with the PhyML tree, with minor statistically unsupported differences, so only the PhyML tree topology is presented.

Results

Subcellular distribution of Miro in Dictyostelium

In *D. discoideum* Miro is encoded by a single gene, *gemA* (Dictybase accession number: DDB_G0267830), localized to chromosome 1. The gene consists of five exons separated by four introns and encodes a protein of 658 amino acids (calculated molecular mass of 75,139.6). The protein displays the typical Miro architecture: two GTPase domains separated by two EF hands, and a transmembrane region at the C-terminus. The regions between the two EF hands and between the second EF hand and the C-terminal GTPase domain are also conserved and have been annotated in Pfam as EF_assoc_2 (PF08356) and EF_assoc_1 (PF08355), respectively, but they do not seem to occur outside Miro proteins (Finn et al., 2010). In the C-terminal GTPase domain the loop connecting the β-strand 5 and α-helix 3 of the standard GTPase fold is expanded by a stretch of 38 residues, almost entirely asparagines (Fig. 1); such low-complexity expansions are a common feature of many *D. discoideum* proteins (Eichinger et al., 2005). The hydrophobic transmembrane sequence is flanked by positively charged residues, as is characteristic for proteins of the outer mitochondrial membrane (Wattenberg and Lithgow, 2001; Borgese et al., 2003). *D. discoideum* Miro displays 33% identity to human Miro1 and Miro2, 29% to *S. cerevisiae* Gem1p and 31% to *D. melanogaster* dMiro.

Author's personal copy

The subcellular localization of Miro in *D. discoideum* cells was investigated using monoclonal antibody K72-624-1 raised against the first GTPase domain. In confocal sections of fixed cells mAb K72-624-1 staining displays a dotted pattern that localizes around the DAPI staining of the mitochondrial DNA (Fig. 2A), indicating that, as already described for other orthologs, *D. discoideum* Miro is a mitochondrial membrane protein. Labeling of cells expressing a GFP fusion of Miro with an antibody that recognizes porin, a protein of the outer mitochondrial membrane (Troll et al., 1992), showed perfect colocalization in ring-like structures (Fig. 2B). Interestingly, neither Miro nor porin appear to be uniformly distributed in the mitochondrial population, suggesting that there are functionally distinct subpopulations of mitochondria. Labeling with the red fluorescent dye MitoTracker Red, which accumulates in the mitochondrial membranes and becomes fluorescent depending on the membrane potential, resulted in dotted structures circumscribed by GFP-Miro. All this is in support of *D. discoideum* Miro being attached to the outer mitochondrial membrane, as has been demonstrated in other species (Frederick et al., 2004; Fransson et al., 2006; Yamaoka and Leaver, 2008).

We used further GFP fusion proteins to investigate which region of Miro is responsible for targeting to the mitochondrial membrane. A GFP fusion of the transmembrane region (amino acids 601–658) displayed a similar pattern of localization as the full-length protein, indicating that the transmembrane region is sufficient for targeting (Fig. 2C). In addition, with this fusion protein a filamentous pattern that interconnects the mitochondria is apparent. The deletion of the transmembrane domain resulted in a disperse localization of the fusion protein throughout the cytoplasm (Fig. 2D), although in some cells a small amount of fusion protein still accumulates at mitochondria, perhaps through unknown direct interactions with proteins of the outer mitochondrial membrane.

Disruption of gemA results in reduced growth

To investigate the function of Miro in vivo, we generated knockout strains (*gemA*$^-$). The *gemA* gene was disrupted by homologous recombination and the recombination event was verified in three independent clones, #5, #6 and #8 (Figure S1). Although no Miro protein was detected in any of the selected clones in Western blots, a weak staining was observed in fixed cells of clone #6 thus clones #5 and #8 were selected for in depth analysis. Because both clones behaved identically, some assays have been performed only in clone #5.

A significant difference was observed between the growth pattern of AX2 and *gemA*$^-$ cells in nutrient medium. AX2 cultures grew with a doubling time of 16 h and reached densities of approximately 11×10^6 cells/ml whereas *gemA*$^-$ cultures of clones #5 and #8 grew with doubling times of 33 h and 38 h and reached densities of 3×10^6 and 4×10^6 cells/ml, respectively (Fig. 3A, left panel). On agar plates with bacteria as a food source however, only a marginal growth defect was observed in the *gemA*$^-$ mutants (Fig. 3B, left panel). To verify that these alterations are solely the result of the Miro deficiency, we transfected *gemA*$^-$ cells with a plasmid that allows constitutive expression of GFP-Miro. Re-expression of Miro reverted the growth defect of *gemA*$^-$ in nutrient medium (Fig. 3A, right panel), but not the altered growth on a bacterial lawn (Fig. 3B, right panel). Failure to improve growth on a bacterial lawn could be a dominant negative effect resulting from expression of GFP-Miro at levels well above the endogenous Miro, because overexpression of GFP-Miro in AX2 cells caused a slight growth defect on bacterial lawn without affecting growth in nutrient medium (Fig. 3A and B, right panels).

The significantly altered growth behavior of the *gemA*$^-$ mutants could result from a defective cell division or a deficient nutrient uptake. To examine a possible defect in cell division, *gemA*$^-$ and AX2 cells grown in shaking suspension were fixed and stained with the DNA-binding dye DAPI for quantification of the number of nuclei per cell. Like AX2, *gemA*$^-$ cells were mainly mono or bi nucleated; indicating that cell division is not affected upon disruption of *gemA* (Figure S2A). Particle and fluid phase uptake were quantified using TRITC-labeled yeast particles and FITC-labeled dextrane, respectively, and were found unaltered in *gemA*$^-$ cells (Figure S2B and C). Release of FITC labeled dextrane was also found unaffected upon disruption of *gemA* (Figure S2D).

Impact of gemA disruption on mitochondrial function

Altered morphology and distribution of mitochondria has been reported in several species upon manipulation of Miro expression (Fransson et al., 2003; Frederick et al., 2004; Yamaoka and Leaver, 2008). In *D. discoideum gemA* deficiency did not result in visible alterations of mitochondrial size (0.50 ± 0.15 μm in *gemA*$^-$ vs. 0.48 ± 0.11 μm in AX2) and morphology. We determined the mitochondrial total mass using MitoTracker Green, which labels the mitochondrial membrane independently from its membrane potential (Pendergrass et al., 2004) and observed a significantly lower value (25%) in *gemA*$^-$ cells compared to wild type cells (Fig. 4A). The cell size was not affected by the disruption of *gemA* (11.65 ± 3.29 μm in *gemA*$^-$ vs. 11.28 ± 3.61 μm in AX2).

Mitochondria convert the energy of nutrient molecules into ATP, which is subsequently provided to cellular reactions. We therefore determined the ATP content in *gemA*$^-$ cells and observed that it was reduced to approximately half compared to wild type cells (0.75 ± 0.53 mol ATP/5×10^6 cells in *gemA*$^-$ vs. 1.6 ± 0.46 mol ATP/5×10^6 cells in AX2) (Fig. 4B). Oxygen consumption was found increased by approximately 40% in *gemA*$^-$ compared to the wild type strain (Fig. 4C). The monosaccharide glucose represents an important energy source for the ATP synthesis. If the mitochondrial function is impaired, one would expect glucose to be catabolized anaerobically, resulting in production of lactate. Glucose consumption and lactate production were therefore investigated. Glucose consumption was found unaltered in *gemA*$^-$ cells (Fig. 4D), whereas no production of lactate was measurable.

The dissipation of the mitochondrial electrochemical potential ($\Delta\psi$) is an early event of apoptosis. Overexpression of human Miro-1 induced an aggregation of the mitochondrial network and resulted in an increased apoptotic rate (Fransson et al., 2003). We determined whether disruption of *gemA* causes alterations in the mitochondrial electrochemical potential using a fluorimetric approach but did not notice any significant difference compared to the wild type strain (Fig. 4E). Mitochondria are also strongly involved in the production of ROS through the electron transporters of the respiratory chain. The cellular ROS production was determined using DCFH-DA staining. Analysis of the relative fluorescence in AX2 and *gemA*$^-$ cells did not reveal significant changes in the formation of reactive oxygen species (Fig. 4F).

Disruption of gemA does not alter processes at the multicellular stage

Van Es et al. described a mitochondrial protein, Tortoise, necessary for efficient chemotaxis in *D. discoideum* (van Es et al., 2001). To determine whether Miro has an influence on this process the chemotactic behavior of *gem A*$^-$ cells was investigated. In the absence of cAMP the *gemA*$^-$ mutants showed a similar behavioral pattern like AX2 cells. Speed, persistence, directionality and directional change were indicative of random movements in both *gemA*$^-$ and AX2 (Table S1). In the presence of cAMP *gemA*$^-$ cells did not differ significantly from wild type cells with respect to speed (12.08 ± 4.86 μm/min in AX2 vs. 12.78 ± 4.74 μm/min in *gemA*$^-$) but directionality was moderately albeit significantly decreased

Author's personal copy

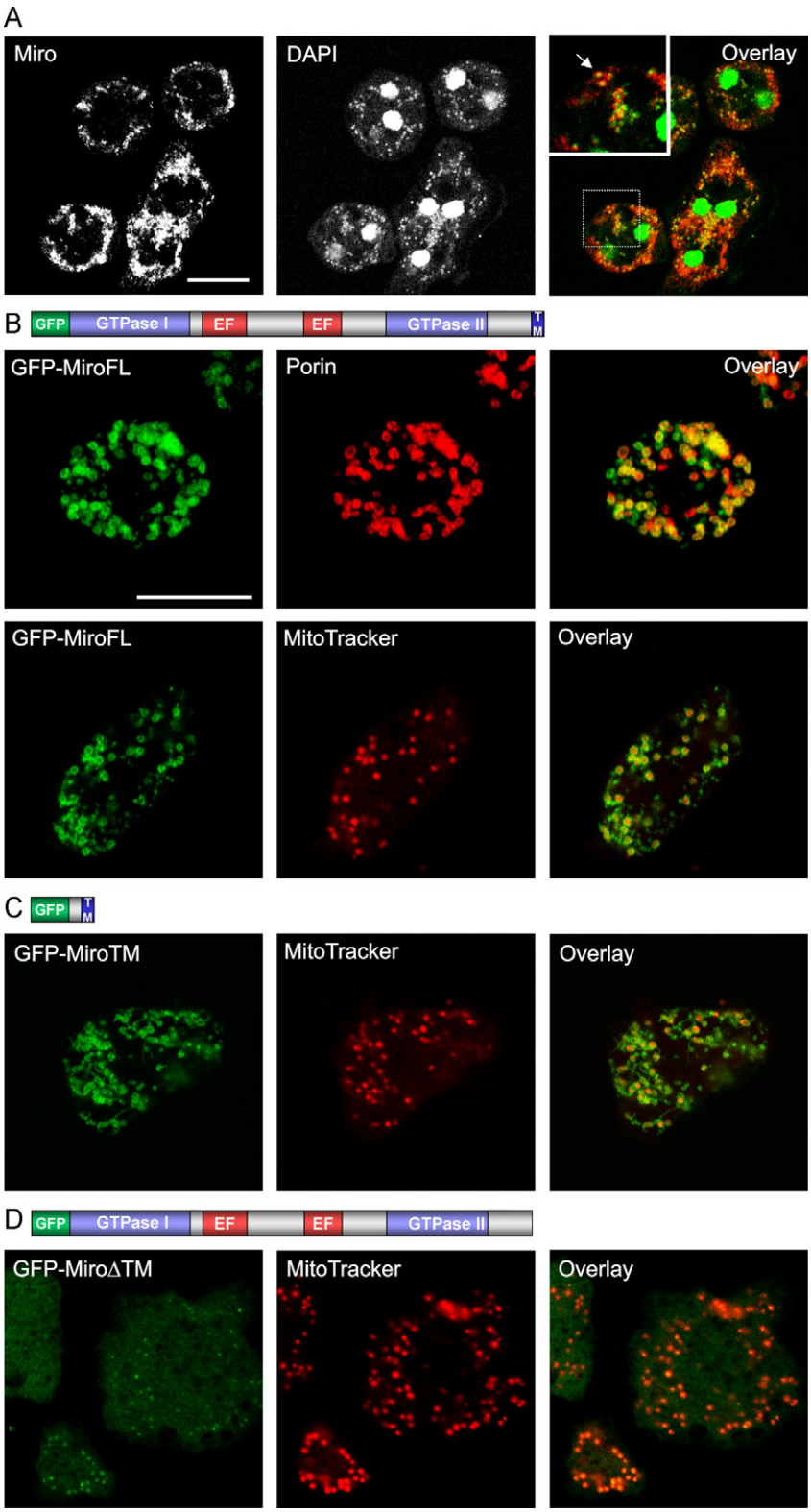

Fig. 2. *D. discoideum* Miro is a mitochondrial membrane protein. (A) *D. discoideum* cells were fixed with methanol and incubated with monoclonal antibody K72-624-1 followed by Cy3 labeled secondary antibody. DAPI was used to visualize nuclei and mitochondrial DNA. The inset shows an enlargement of the indicated region. The arrow marks a group of mitochondria with Miro shown in red and DNA in green. Scale bar, 10 μm. (B) Miro colocalizes with mitochondrial membrane markers. In the upper panels GFP-Miro expressing *D. discoideum* cells were fixed with methanol and incubated with an antibody against porin, a protein of the outer mitochondrial membrane, followed by Cy3 labeled secondary antibody. In the lower panels cells were stained with MitoTracker Red and fixed with paraformaldehyde/picric acid. GFP-Miro is seen as ring-shaped structures. (C) The transmembrane domain is sufficient for anchoring of the protein to the mitochondrial membrane. Cells expressing a GFP fusion of the transmembrane domain were processed as in B for MitoTracker Red staining. (D) The transmembrane domain is necessary for targeting Miro to the mitochondrial membrane. Cells expressing a GFP fusion of a truncated Miro lacking the transmembrane domain were processed as in A for MitoTracker Red staining. The fusion protein is diffusely distributed throughout the cytoplasm. Images were taken with a confocal laser scanning microscope. Scale bar for B, C and D, 10 μm. (For interpretation of the references to color in this figure legend, the reader is referred to the web version of the article.)

Author's personal copy

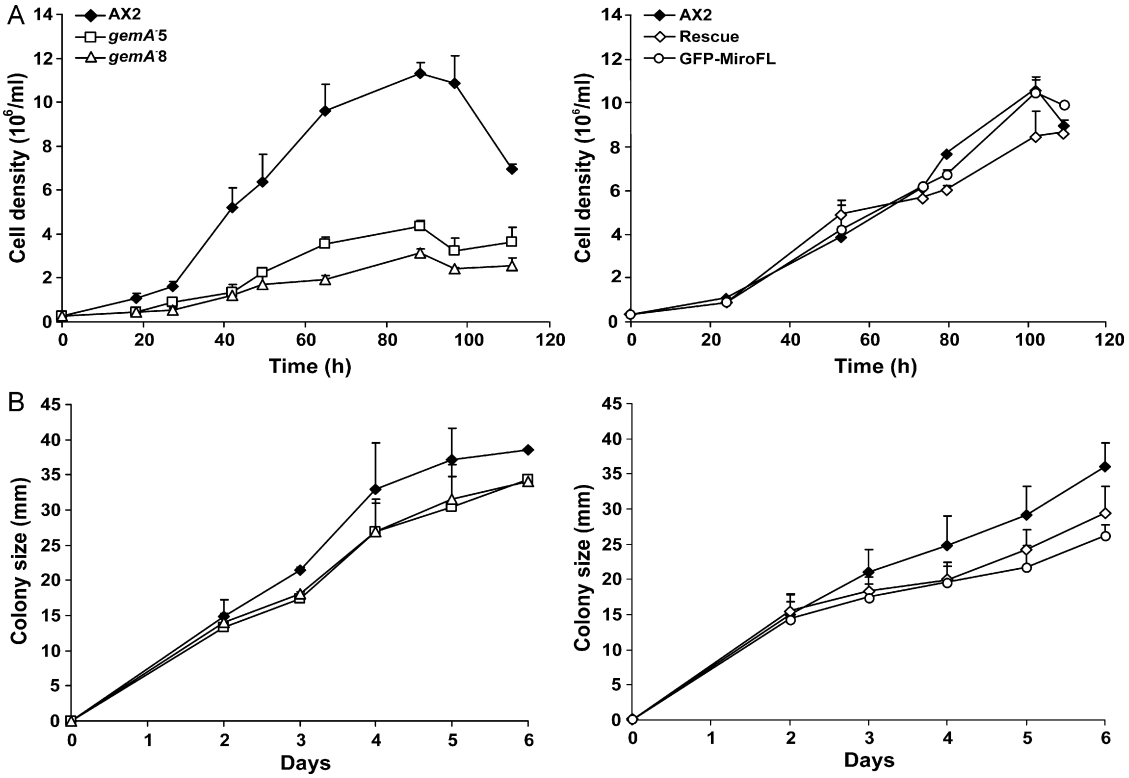

Fig. 3. Effects of deficiency and overexpression of Miro on growth. (A) Growth in suspension of AX2, two independent *gemA*$^-$ clones, a *gemA*$^-$ strain re-expressing Miro (rescue) and an overexpressor strain (AX2 expressing GFP-Miro). Cultures were inoculated at a cell density of 0.25×10^5 cells/ml and cell density determined at the indicated time points. Growth of *gemA*$^-$ cells (left panel) is considerably impaired, but the defect is overcome by reintroduction of Miro. Overexpression of Miro does not affect the growth rate. (B) Growth on a bacterial lawn. 15 μl of cell suspension was deposited in the middle of a *K. aerogenes* lawn. The diameter of the colony was measured after 48 h and every following day. Shown are average and standard deviation of three independent series of measurements. For clarity, error bars are depicted in one direction only.

(0.81 ± 0.09 in AX2 vs. 0.66 ± 0.16 in *gemA*$^-$). Both strains polarized, formed streams and migrated in the direction of the cAMP source.

Disruption of another mitochondrial protein, MidA, causes alterations in the developmental pattern of *D. discoideum* (Torija et al., 2006). We therefore investigated the formation of aggregation streams of *gemA*$^-$ cells during starvation on a plastic surface under a liquid film. The typical spiral pattern formation started 4 h after the onset of starvation and was observed in AX2 as well as in *gemA*$^-$, indicating that the cAMP relay is not impaired in the *gemA*$^-$ strain. Although in *gemA*$^-$ streams were occasionally thinner and at times broke, a significantly delayed aggregation was not observed (Fig. 5A). We monitored the complete developmental cycle of *gemA*$^-$ on non-nutrient agar plates and did not notice differences in timing of development or in the shape and size of the multicellular structures. Both *gemA*$^-$ and AX2 produced fully developed fruiting bodies (Fig. 5B). To investigate possible subtle morphological alterations in the developmental stages we determined the expression of contact site A (CsA), an aggregation stage specific cell adhesion protein. We observed that CsA is expressed with a delay of up to 3 h in *gemA*$^-$ (Fig. 5C). Finally, mitochondrial proteins have been implicated in the process of phototaxis (Kotsifas et al., 2002; Bokko et al., 2007). The phototactic behavior of *gemA*$^-$ slugs was examined but was not found to differ from that of AX2 (Fig. 5D).

Distribution of mitochondria depends on an intact microtubule network but does not require Miro

In mammals long distance transport of mitochondria occurs along microtubules while actin provides tracks for short range transport to areas which the microtubules do not reach. In plant cells and yeast transport of mitochondria takes place primarily on actin filaments (Frederick and Shaw, 2007). The mitochondrial transport mechanisms that operate in *D. discoideum* have not been investigated extensively, although there is evidence that mitochondria are transported along microtubules (Fields et al., 2002). Although difficult to document in fixed cells, mitochondria can be found associated to microtubules. This is more clearly evident in large protrusions of cells attached to a substrate. Here a few mitochondria are retained attached to the microtubules running along the protrusion (Fig. 6A). The displacement of mitochondria along microtubules in vivo is also difficult to document because apparently only a few mitochondria are attached to microtubules at a given time and they easily move out of the focal plane (see supplementary movies). Fig. 6B shows some frames of a time series in which a single mitochondrion displaces towards the periphery along a microtubule. At time frame 35″ the microtubule appears to have detached from the cell periphery but the mitochondrion remains attached near the microtubule tip.

We performed indirect immunofluorescence studies and live image microscopy to investigate the effects of treatment with drugs that disrupt the microtubule or the actin network on the distribution of mitochondria and whether the depletion of Miro has any impact on the pattern of mitochondrial distribution. In untreated vegetative cells mitochondria appear dispersed all over the cell, except the area occupied by the nucleus and the microtubule organizing center (MTOC). Clusters of mitochondria are apparent occasionally. Immunostaining with a tubulin antibody shows numerous curved microtubules stretching out of the MTOC toward the cell periphery. The mitochondrial distribution did not differ appreciably between *gemA*$^-$ and wild type cells (Fig. 7, first row panels).

Treatment with nocodazole resulted for the most part in a degraded microtubule network, with the MTOC remaining visi-

Author's personal copy

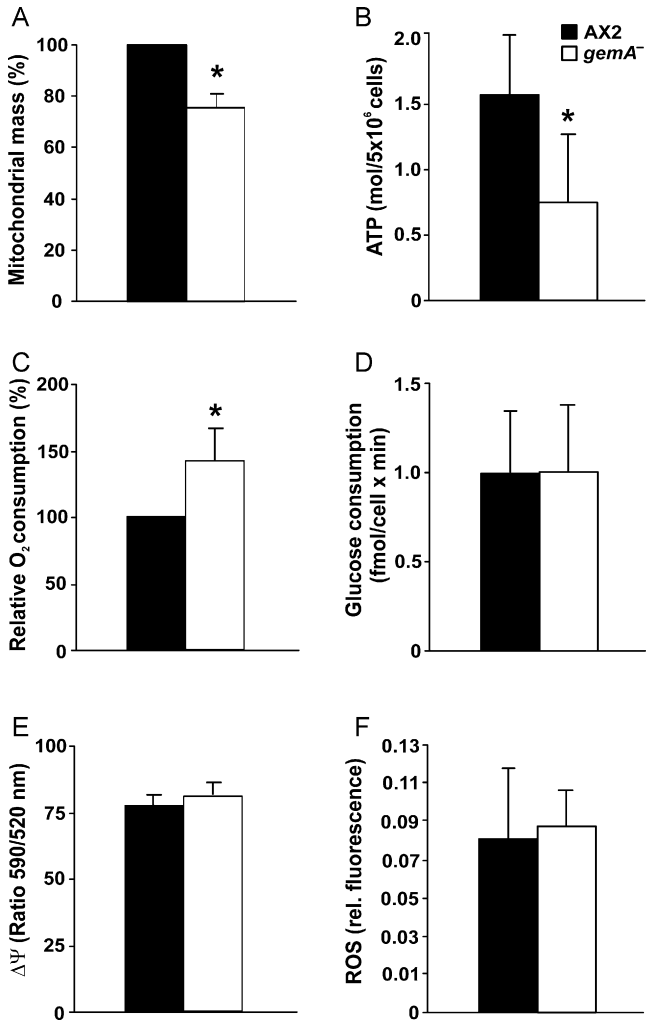

Fig. 4. Miro deficiency impacts on mitochondrial metabolism. (A) Mitochondrial mass of axenically grown cells was determined after incubation with 200 nM MitoTracker Green. In *gemA*$^-$ the mitochondrial total mass is reduced by approximately 25%. Data are the average and standard deviation of five independent series of measurements. $^*p \leq 0.001$, Student's *t*-test. (B) The ATP content of axenically grown cells was determined with a luciferase-based method. The ATP content is reduced by more than 2-fold in *gemA*$^-$. Data are the average and standard deviation of two independent series of measurements. $^*p \leq 0.001$, Student's *t*-test. (C) Oxygen consumption was measured using a Clark-type oxygen electrode in a respiration chamber for 5–10 min after equilibration of the electrode. Oxygen consumption was 40% higher in *gemA*$^-$. Data are the average and standard deviation of six independent series of measurements. $^*p \leq 0.001$, Student's *t*-test. (D) Glucose consumption. Cultures were inoculated at a cell density of 3×10^6 cells/ml, the glucose content was determined in the supernatant at 24 h intervals and the glucose consumption was calculated related to the cell density. Data are the average and standard deviation of two independent series of measurements. (E) Electrochemical potential. Exponential growth phase cells were stained with 200 nM JC-1 for 30 min at 21 °C in the dark. After washing, the ratio of fluorescence emission at 590 and 520 nm at excitation 488 nm was determined. Data are the average and standard deviation of two independent series of measurements each with 20–30 samples. (F) Reactive oxygen species production. Axenically grown cells were incubated with 100 nM DCFH-AA in the dark. After washing, the fluorescence emission at 525 nm at excitation 490 nm was determined. Data are the average and standard deviation of two independent series of measurements each with 20–30 samples.

ble and tubulin accumulating in disperse spot-like structures, but actin distribution and cell morphology remained mainly unaltered. Nocodazole caused increased clustering of mitochondria at the periphery of the cell in both *gemA*$^-$ and wild type cells (Fig. 7, second row panels). Disruption of the microfilament network with cytochalasin A or latrunculin B caused, besides alterations of the cell morphology and actin distribution, profound alterations of the microtubule network too. Whereas in cells treated with cytochalasin A the MTOC was displaced to the cell periphery, where it remained connected to bundles of microtubules (Fig. 7, third row panels), treatment with latrunculin B resulted in a pattern that resembled the effect of nocodazole on the microtubule network (Fig. 7, fourth row panels). In both cases the mitochondria appeared more clustered, predominantly at the cell periphery, and *gemA*$^-$ and wild type cells behaved identically. The effects of these drugs in AX2 cells in vivo can be observed in supplemental movies 1 (nocodazole), 2 (cytochalasin A) and 3 (latrunculin B). All three drugs caused an arrest of mitochondrial movements, disassembly of the microtubule network, and a variable extent of clustering of mitochondria. *GemA*$^-$ cells behaved identically upon drug treatment. Collectively these results indicate that in *D. discoideum* the distribution of mitochondria depends on an intact microtubule network and that Miro does not play an essential role in maintaining mitochondrial morphology and distribution.

In an attempt to quantify mitochondrial motility in living cells we acquired time lapse movies of AX2 and *gemA*$^-$ cells at 2 s intervals. Cells were overlaid with a thin sheet of agarose in order to achieve larger numbers of mitochondria within a focal plane. Supplemental movies 3 (AX2) and 4 (*gemA*$^-$) show that most mitochondria undergo short movements and only occasionally a few mitochondria display longer range smooth displacements compatible with transport along microtubules. Frequently mitochondria can be observed in clusters of various sizes. Attempts at reliably quantifying mitochondrial motility in living cells were hampered by this heterogeneity and by the fact that an important component of organelle movements is attributable to streaming of cytoplasm during formation of protrusions and during cell displacement. No noticeable differences between *gemA*$^-$ and AX2 cells were apparent in the behavior of mitochondria in vivo.

We next explored a possible association of Miro to kinesins. The kinesin family is composed of 13 genes in *D. discoideum*. Four kinesins, Kif1, Kif3, Kif5 and Kif7, belong to the class of organelle transporters (Kollmar and Glockner, 2003). Kif5 is the most similar to human conventional kinesins and is the most likely candidate for binding a putative KLC. It therefore appears as a likely candidate for associating to Miro. We immunoprecipitated GFP-fused Miro and probed for the presence of Kif5 in the immune complexes but were not able to detect this kinesin (Figure S3).

Structural diversity and evolution of the Miro family

In order to understand the function of Miro proteins in a wider phylogenetic context, we searched for homologs in a set of currently available genomic sequences from diverse species representing most major eukaryotic lineages (Table S2). At least one Miro gene could be found in almost all eukaryotes, with only a few exceptions (Figure S4). First, Miro is apparently absent from all eukaryotes with mitosomes or hydrogenosomes in place of "classical" mitochondria, including Microsporidia, *Entamoeba* spp., *Giardia intestinalis*, and *Trichomonas vaginalis*. Second, Miro seems to be absent from genomes of some lineages that generally do exhibit aerobic mitochondria, such as Myzozoa (all apicomplexans and *Perkinsus marinus*), green algae of the order Mamiellales (*Ostreococcus* spp. and *Micromonas* spp.), the haptophyte *Emiliania huxleyi*, and the stramenopile alga *Aureococcus anophagefferens*. Although some of these genomes remain incomplete, Miro homologs are not discernible in EST sequences from these species, too, indicating that the lack of Miro genes may be genuine.

To highlight the structural diversity of Miro proteins, we constructed a multiple alignment (Figure S5). Most of them retain the architecture described previously for metazoan, fungal, and plant Miro proteins, i.e., two GTPase domains separated by two EF hands

Author's personal copy

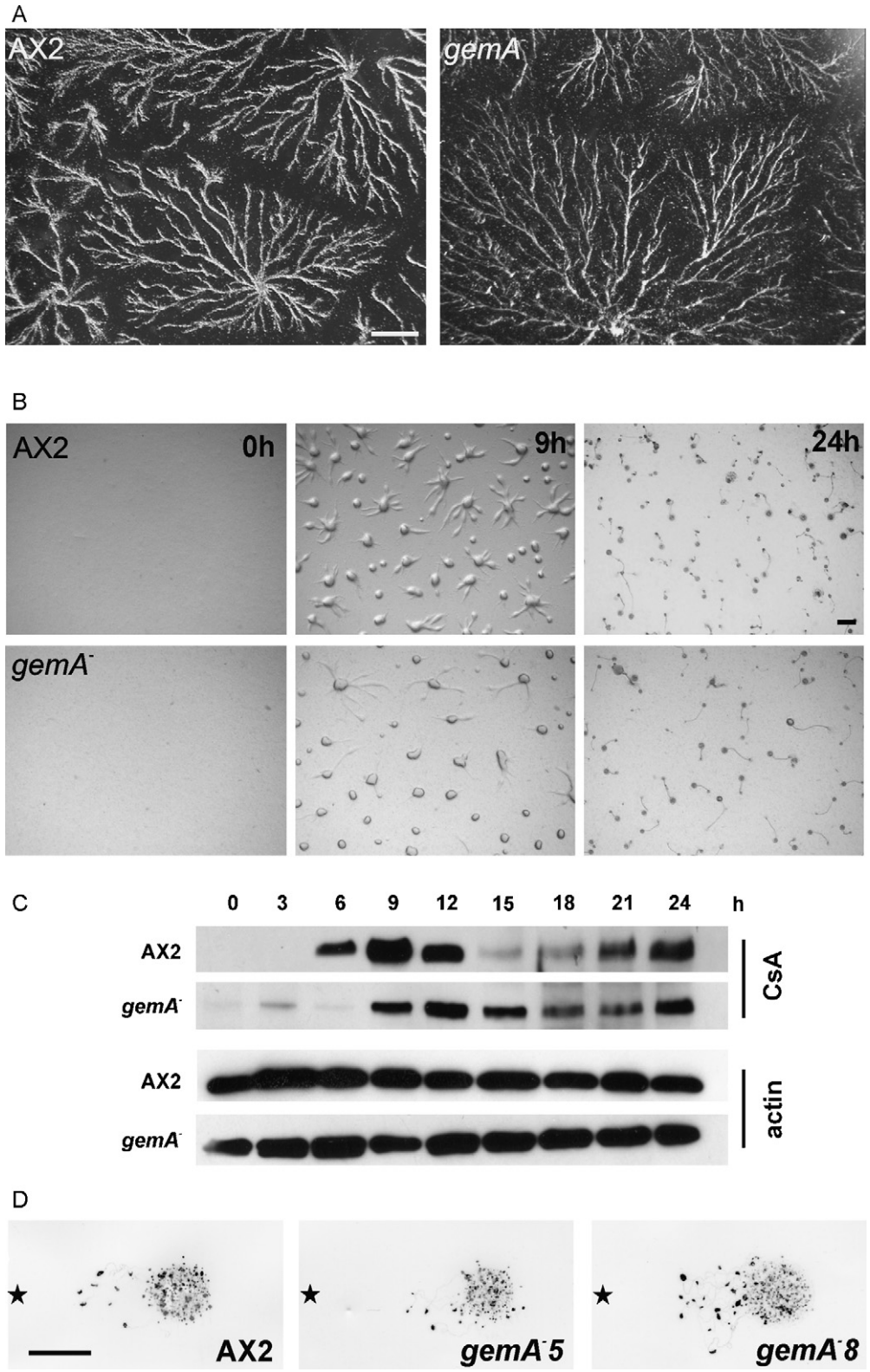

Fig. 5. The multicellular stage of the life cycle is unaffected in the *gemA*$^-$ mutant. (A) Aggregation on a plastic surface. Cells were starved submerged in Soerensen buffer at a density of 2×10^5 cells/cm^2 on plastic plates and monitored for aggregation. Shown are images taken 10 h after the onset of starvation. Bar, 1 cm. (B) Development on phosphate agar. Axenically growing cells were washed in Soerensen buffer, plated at a cell density of 5×10^6 cells/cm^2 on a phosphate agar plate and incubated at 21 °C. Images were taken with a stereomicroscope at the indicated time points. Bar, 1 mm. (C) Expression pattern of the developmental marker contact site A. Cell lysates of 4×10^5 cells were loaded on a 10% SDS polyacrylamide gel, transferred onto nitrocellulose membrane and probed with csA specific monoclonal antibody followed by peroxidase-coupled anti-mouse antibody and enhanced chemiluminescence. Actin was used as loading control. (D) Phototaxis. Axenically growing cells were washed in Soerensen buffer and 1×10^6 cells were placed on the center of a water agar plate. The plates were then placed in a dark box with a 3 mm slit at 21 °C for 48 h. Multicellular structures were transferred to nitrocellulose membranes and slugs and their slime trails were stained with amido black. The star on the left hand side marks the direction of the light source. Bar, 1 cm.

Author's personal copy

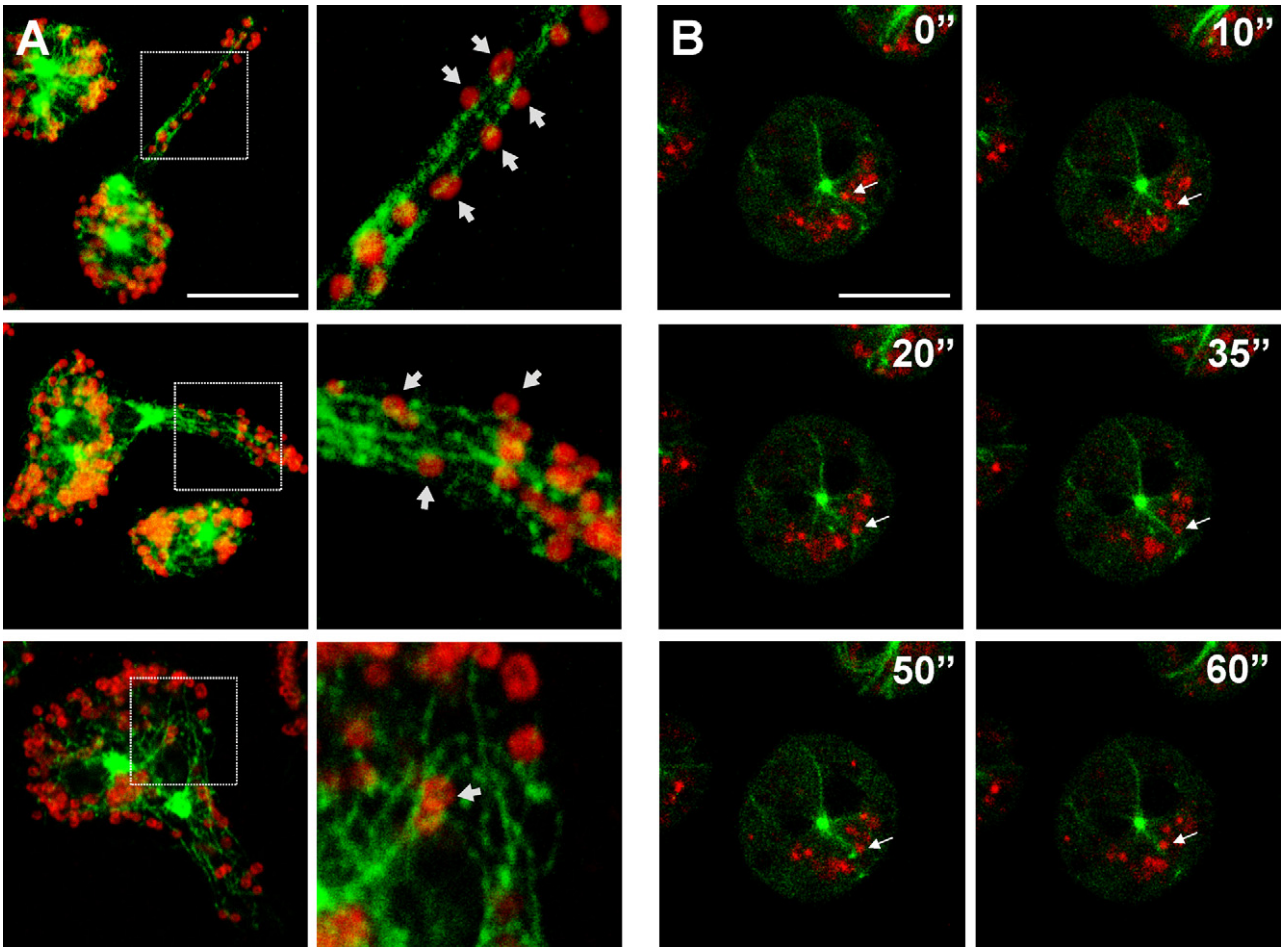

Fig. 6. Mitochondria associate with the microtubule network. (A) *D. discoideum* cells were fixed with methanol and incubated with an antibody against porin (in red) followed by anti-mouse Alexa 647 labeled secondary antibody. Tubulin (in green) was stained with YL1/2 antibody followed by anti-rat Alexa 488 labeled secondary antibody. Panels on the right hand side of each image are enlargements of the indicated regions. Arrows mark examples of mitochondria placed next to a microtubule. Images were taken with a confocal laser scanning microscope. Scale bar, 10 μm. (B) In vivo behavior of mitochondria. Cells expressing GFP-tubulin were allowed to adhere on a coverslip and were stained with MitoTracker Red prior to live imaging with a confocal laser scanning microscope. Frames at the indicated times were selected from a time series. Arrows mark a mitochondrion displacing along a microtubule. Scale bar, 10 μm. (For interpretation of the references to color in this figure legend, the reader is referred to the web version of the article.)

and a C-terminal transmembrane region. There are, however, several notable deviations from this domain organization (Fig. 8A). The most unusual are Miro proteins from the trypanosomatid flagellates (*Trypanosoma* spp. and *Leishmania* spp.), which appear to lack the otherwise highly conserved N-terminal GTPase domain. They instead exhibit a novel N-terminal domain of approximately 120 amino acid residues that does not show any apparent homology to the GTPase or any other defined domain as evaluated using the sensitive PSI-BLAST (Altschul et al., 1997) or HHpred (Soding et al., 2005) searches. Another unusual Miro structure is found in ciliates of the class Oligohymenophorea, for which genome sequences are available, and concerns the region normally occupied by the C-terminal GTPase domain: it lacks all GTPase-specific motifs and is poorly conserved even among ciliate species. It is possible that this region represents a deteriorated GTPase domain that conserves some role in supporting the structure of the rest of the protein.

Some species exhibit less pronounced yet potentially functionally important departures, like low complexity insertions of varying length at different positions of the protein (Figure S4). In trypanosomatids Miro is unusual in that it has a deletion of eight out of twelve residues of the Ca^{2+}-binding loop within the second EF hand motif, casting doubt on its functionality. Further disruptions of conserved motifs are apparent in the C-terminal GTPase domain of some Miro proteins, for example in the phosphate-binding P-loop (G1 motif) in *Acanthamoeba castellanii* or in the [N/T]KxD (i.e., G4) motif in some Amoebozoa and Stramenopiles. It is possible that GTP binding and/or hydrolysis are negatively affected by these mutations.

A maximum likelihood phylogenetic tree of Miro protein sequences (excluding the unusual ones from trypanosomatids and ciliates) shows a very good concordance with the species phylogeny (Fig. 8B). Most major eukaryotic groups are recovered as monophyletic, with the exception of the Amoebozoa, since the sequence from *A. castellanii* does not cluster together with Miro from the remaining amoebozoans but is placed on a neighboring branch together with a sequence from the apusomonad *Amastigomonas* sp. ATCC 50062. Given the general difficulties in obtaining monophyletic Amoebozoa in other single-gene trees (Pawlowski and Burki, 2009), this branching pattern is not too surprising. Our tree further sheds light on the origin of the multiple Miro paralogs possessed by some species (see Figure S3 for details).

Discussion

Miro proteins characterized so far are anchored to the outer mitochondrial membrane and the *D. discoideum* ortholog is no exception. We also show that the C-terminal transmembrane region is both necessary and sufficient for anchoring to the outer mitochondrial membrane, as previously reported for the yeast,

Author's personal copy

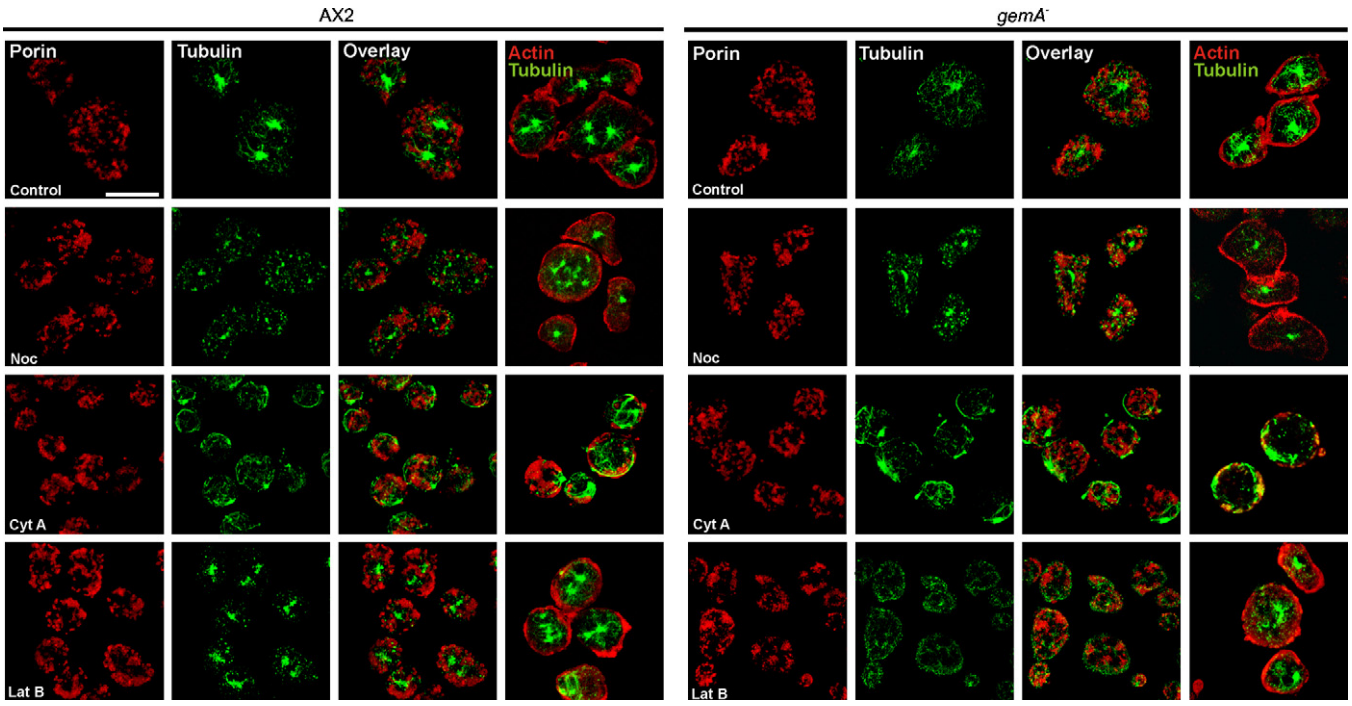

Fig. 7. Disruption of the microtubule network results in aggregation of mitochondria. Cells were fixed with methanol after treatment with nocodazole (30 μg/ml, 3 h), cytochalasin A (20 μM, 1 h) or latrunculin B (2 μM, 45 min) and incubated with an antibody against porin (in red) followed by anti-mouse Alexa 647-labeled secondary antibody. Tubulin (in green) was stained with YL1/2 antibody followed by anti-rat Alexa 488-labeled secondary antibody. Actin (in red) was stained with Act 1-7 antibody followed by anti-mouse Alexa 647-labeled secondary antibody. Treatment with nocodazole disrupts the microtubule network without noticeably affecting the actin distribution, whereas disruption of the actin cytoskeleton results in altered tubulin distribution as well. All treatments cause aggregation of mitochondria. Images were acquired with a confocal laser scanning microscope. Bar, 10 μm. (For interpretation of the references to color in this figure legend, the reader is referred to the web version of the article.)

human and plant orthologs (Frederick et al., 2004; Fransson et al., 2006; Yamaoka and Leaver, 2008). To investigate the roles of Miro in *D. discoideum* we have generated knockout and overexpressor cell lines and have examined mitochondrial processes and other processes that are affected by mitochondrial functioning in *D. discoideum*. A disruption of *gemA* did not lead to obvious alterations in the size, morphology and distribution of mitochondria, though *gemA*$^-$ cells showed a significantly lower mitochondrial mass. In contrast to that, the deficiency of Miro as well as the overexpression of particular mutants in human cells, yeast and *Drosophila* led to distinct alterations in the mitochondrial morphology and distribution. In human cells the formation of threadlike and closely packed mitochondria has been reported in overexpressors (Fransson et al., 2006), whereas in yeast a Miro deficiency leads to collapsed, globular or grapelike mitochondria (Frederick et al., 2004). In *Drosophila* both loss and overexpression of dMiro alter the length of mitochondria in axons (Russo et al., 2009) and the loss of dMiro led to abnormal subcellular distribution of mitochondria in nerves and muscles, with accumulation in the soma and absence in the neuromuscular junctions (Guo et al., 2005).

From a functional viewpoint the most dramatic alteration observed in the *gemA*$^-$ mutant was a growth defect in nutrient medium, a defect also observed in the yeast mutant (Frederick et al., 2004). This defect is not due to impaired cytokinesis or endocytosis, which are frequent causes of growth defects in *D. discoideum*, but can be attributed rather to a mitochondrial dysfunction. Miro deficiency resulted in a reduction of the amount of ATP to approximately half of the wild type content. This change cannot be explained by a decreased mitochondrial mass only, as this was reduced only marginally. By contrast, the rate of oxygen consumption was found to be significantly higher in *gemA*$^-$ cells, although the rate of glucose consumption was not altered. The increased rate of oxygen consumption may constitute a compensatory mechanism to the reduced ATP content, but taken collectively the functional data indicate an inefficient processing of fuel molecules by the mitochondria. The defect is not compensated by increased lactate production, in agreement with *D. discoideum* being considered an exclusively aerobic organism (Schiavo and Bisson, 1989). Interestingly, necrotic cell death in *D. discoideum* is characterized by ATP depletion and increased oxygen consumption. However, this is accompanied by perinuclear clustering of dilated mitochondria (Laporte et al., 2007), an alteration that we do not observe in *gemA*$^-$ cells. Further studies have shown that mitochondrial proteins influence processes like phototaxis (Kotsifas et al., 2002), chemotaxis (van Es et al., 2001) and development (Torija et al., 2006) in *D. discoideum*. None of those was found altered in *gemA*$^-$, therefore we conclude that Miro is not part of the signal transduction pathways that regulate the multicellular phase of the *D. discoideum* life cycle.

Because Miro proteins have emerged as key regulators of microtubule-dependent mitochondrial transport, we examined this aspect in *D. discoideum*. Very few studies have addressed the mitochondrial transport mechanisms that operate in this organism. Using microfilament or microtubule disrupting drugs it was concluded in a previous report that neither the actin cytoskeleton nor the microtubule network plays a major role on the distribution of mitochondria (Fields et al., 2002). Using concentrations of nocodazole higher than in that report, we observe an arrest of mitochondrial movements and clustering of mitochondria, predominantly at the periphery of the cell. Interestingly, disruption of the actin filament network has a similar effect because it causes a concomitant disruption of the microtubule network. This is due to the fact that microtubule tips are anchored to cortical actin filaments (Hestermann et al., 2002). Because nocodazole does not cause dramatic changes in the pattern of actin distribution, we conclude that in *D. discoideum* mitochondria rely on the microtubule network at least for some displacements. Mitochondria can be seen associated to microtubules and in agreement with a previous report (Fields et al., 2002), we have observed occasional transport of mito-

Author's personal copy

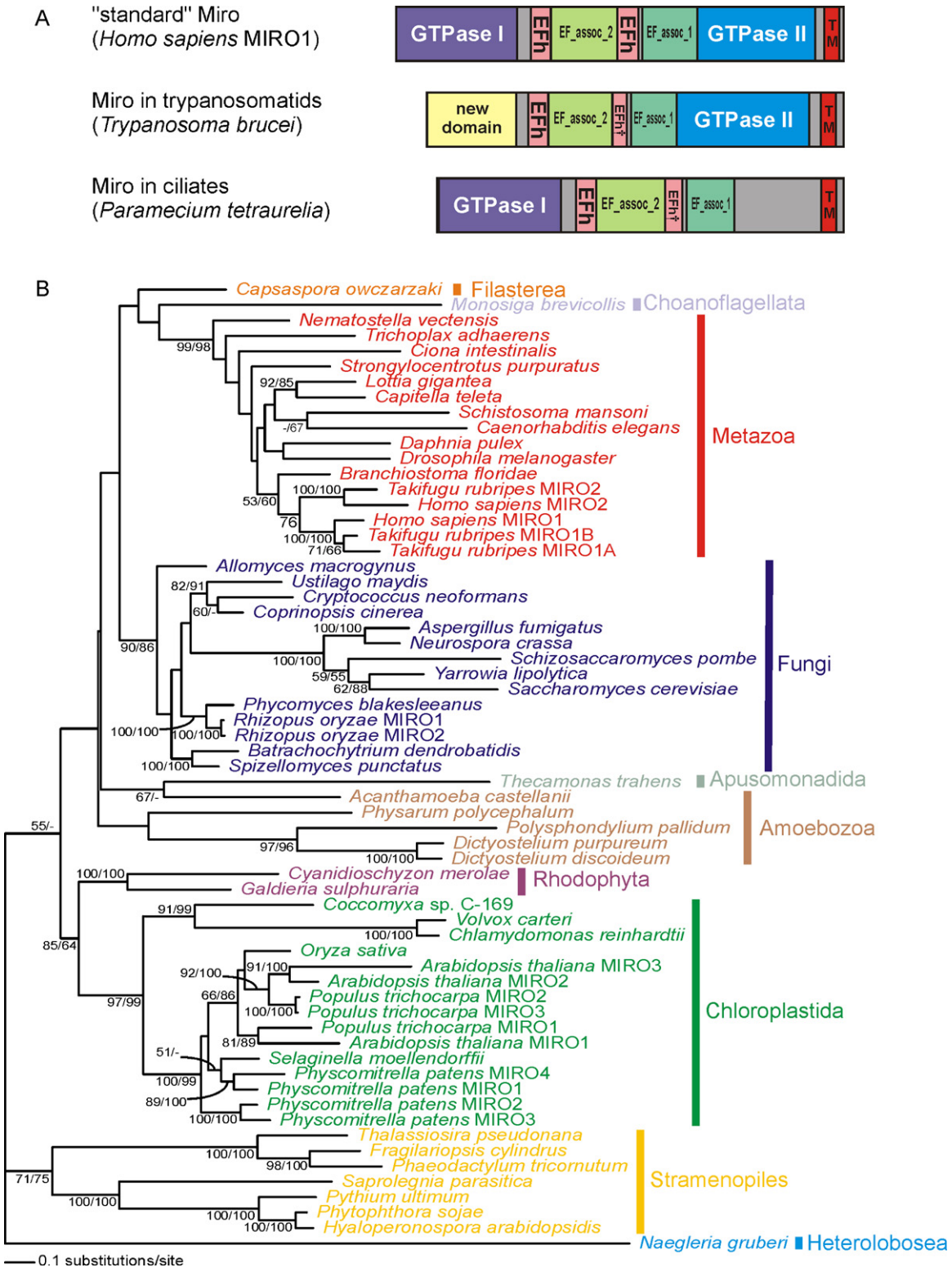

Fig. 8. Evolution and domain architecture of the Miro family. (A) Domain architectures of Miro proteins. The domains and their boundaries are drawn based on results from SMART and Pfam searches and inspection of a multiple alignment of Miro sequences. The second EF hand (EFh) motif in trypanosomatid and ciliate proteins (marked with a crosslet) is disrupted by a deletion or mutations, respectively, and its functionality is uncertain. (B) Maximum likelihood phylogenetic analysis of Miro protein sequences. The tree was inferred using the PhyML 3.0 and JTT+Γ4+I substitution model. Bootstrap values (shown when higher than 50%) were calculated using the PhyML/RAxML rapid bootstrapping algorithm. Accession numbers of the sequences included in the analysis are provided in Table S2.

chondria along microtubules in vivo. Although we cannot formally exclude that some actin-dependent mitochondrial transport takes place in *D. discoideum*, it is likely to be inefficient, considering that in this organism the actin cytoskeleton does not provide long tracks, but is organized as a mainly cortical network of relatively short filaments (Diez et al., 2005).

Although mitochondria occasionally use microtubules for transport in *D. discoideum*, it appears that Miro does not play a major role

Author's personal copy

in this process, judging from the unaltered pattern of mitochondrial distribution and movements in the *gemA*$^{-}$ mutant. The exact roles of *D. discoideum* kinesins in mitochondrial transport have not been investigated in sufficient detail. Mitochondrial motility has been found unaltered in Kif1/Unc104 deficient cells. This kinesin is the dominant plus-end-directed motor for vesicle transport (Pollock et al., 1999). Of the three KHC kinesins of *D. discoideum* Kif7 is an unlikely candidate for mitochondrial transport, as this protein is only present at late stages of development (de Hostos et al., 1998). Kif3 co-localizes with vesicular structures, but apparently not with mitochondria. Biochemically and in terms of sequence similarity Kif3 resembles fast fungal kinesins, that reportedly do not participate in mitochondrial transport (Röhlk et al., 2008). We show here that Miro does not associate to Kif5, a kinesin that binds actin filaments through its tail and accumulates at actin-rich protrusions (Iwai et al., 2004). Although further studies are needed to rule out that any of the mentioned kinesins might associate transiently with mitochondria, Miro does not appear to be required to mediate that association.

We propose that in *D. discoideum*, as in yeasts and plants, Miro plays an important role unrelated to mitochondrial transport. The ability to build a complex that regulates the association of Miro to kinesin for microtubule-dependent transport probably arose in metazoans. This innovation makes sense particularly in neurons, where mitochondria need to be efficiently transported over very long distances. Consequently, defects in Miro or Milton have profound consequences for the distribution of mitochondria in these cells and for activities that require appropriate energy supply in the synaptic endings (Guo et al., 2005; Glater et al., 2006). In support of this hypothesis, it is noteworthy that none of the components reported in mammals and *Drosophila* as interacting partners of Miro for regulation of binding to KHC, like Milton and the Milton-related proteins GRIF-1 and OIP106, or Pink1, is present in *D. discoideum* (our own database search), yeasts or plants (Yamaoka and Leaver, 2008). Miro-related proteins compete with KLC for binding to KHC and it is noteworthy that no KLCs have been identified in *D. discoideum*. The ancestral role of Miro is apparently related to aspects of mitochondrial homeostasis not related to transport, as shown here in the *D. discoideum* mutant. Alterations of this ill-defined Miro function would also explain the morphological alterations reported in the yeast and plant mutants (Frederick et al., 2004; Yamaoka and Leaver, 2008), but also the effects on apoptosis described in mammalian cells (Fransson et al., 2003) and the reduced mitochondrial ATP production reported in dMiro mutated flies (Guo et al., 2005). In this context future studies aimed at identifying additional interaction partners will provide further insight into the mechanism by which Miro GTPases regulate mitochondrial homeostasis.

Our paper is the first to assess the actual distribution and structural diversity of Miro in a broader phylogenetic context. Since there are no direct homologs discernible in prokaryotes, Miro must be regarded as a eukaryotic innovation. In addition, the presence of Miro in at least some representatives of all major eukaryotic lineages and the predominantly, if not exclusively, vertical inheritance of Miro genes implies that Miro evolved in the earliest stages of eukaryotic evolution, perhaps before the divergence of extant eukaryotes. Together with its physical and functional association with the mitochondrion, it seems reasonable to suggest that the Miro advent was one of the fundamental steps in the evolutionary path from the alphaproteobacterial endosymbiont to a fully-fledged mitochondrion. Some lineages subsequently lost Miro hand-in-hand with the overall reduction and modification of their mitochondria converting them to mitosomes and hydrogenosomes. The apparent absence of Miro from some organisms presumably possessing "standard" aerobic mitochondria (Mamiellales, *Emiliania*, *Aureococcus*) is striking and suggests that these mitochondria might be unusual in some way.

The domain architecture previously identified in metazoan, fungal, and plant Miro proteins is conserved in most eukaryotes and thus may represent the ancestral state, whereas the non-canonical versions, including that in trypanosomatids, are most likely lineage-specific derivations. However, it is interesting to note that a recently proposed hypothesis places the root of the eukaryotic tree between Euglenozoa (including trypanosomatids) and the remaining eukaryotes (Cavalier-Smith, 2009), raising the possibility that the unique arrangement of the N-terminus in the trypanosomatid Miro is primary. The characterization of Miro from other euglenozoans (bodonids, diplonemids, euglenids) may help resolve this question.

Acknowledgments

We thank Angelika A. Noegel for continuous generous support, Berthold Gassen for providing monoclonal antibodies, Ann Kathrin Meyer for technical support and Kazuo Sutoh for providing Kif5 antiserum. This work was supported by the Deutsche Forschungsgemeinschaft, the Köln Fortune Program of the Medical Faculty, University of Cologne and the Käthe-Hack, Imhoff, and Maria-Pesch foundations. ME was supported by project no. P305/10/0205 of the Czech Science Foundation.

Appendix A. Supplementary data

Supplementary data associated with this article can be found, in the online version, at doi:10.1016/j.ejcb.2010.10.012.

References

Abo, A., Pick, E., Hall, A., Totty, N., Teahan, C.G., Segal, A.W., 1991. Activation of the NADPH oxidase involves the small GTP-binding protein p21^{rac1}. Nature 353, 668–670.

Adachi, H., Hasebe, T., Yoshinaga, K., Ohta, T., Sutoh, K., 1994. Isolation of *Dictyostelium discoideum* cytokinesis mutants by restriction enzyme-mediated integration of the blasticidin S resistance marker. Biochem. Biophys. Res. Commun. 205, 1808–1814.

Altschul, S.F., Madden, T.L., Schaffer, A.A., Zhang, J., Zhang, Z., Miller, W., Lipman, D.J., 1997. Gapped BLAST and PSI-BLAST: a new generation of protein database search programs. Nucleic Acids Res. 25, 3389–3402.

Ausubel, F.M., Kingston, R.E., Moore, D.D., Seidman, J.G., Smith, J.A., Struhl, K., 2001. Current Protocols in Molecular Biology. John Wiley & Son, Inc., New York, USA.

Bertholdt, G., Stadler, J., Bozzaro, S., Fichtner, B., Gerisch, G., 1985. Carbohydrate and other epitopes of the contact site A glycoprotein of *Dictyostelium discoideum* as characterized by monoclonal antibodies. Cell Differ. 16, 187–202.

Bokko, P.B., Francione, L., Bandala-Sanchez, E., Ahmed, A.U., Annesley, S.J., Huang, X., Khurana, T., Kimmel, A.R., Fisher, P.R., 2007. Diverse cytopathologies in mitochondrial disease are caused by AMP-activated protein kinase signaling. Mol. Biol. Cell 18, 1874–1886.

Borgese, N., Brambillasca, S., Soffientini, P., Yabal, M., Makarow, M., 2003. Biogenesis of tail-anchored proteins. Biochem. Soc. Trans. 31, 1238–1242.

Cavalier-Smith, T., 2009. Kingdoms Protozoa and Chromista and the eozoan root of the eukaryotic tree. Biol. Lett. 6, 342–345.

de Hostos, E.L., McCaffrey, G., Sucgang, R., Pierce, D.W., Vale, R.D., 1998. A developmentally regulated kinesin-related motor protein from *Dictyostelium discoideum*. Mol. Biol. Cell 9, 2093–2106.

Diez, S., Gerisch, G., Anderson, K., Müller-Taubenberger, A., Bretschneider, T., 2005. Subsecond reorganization of the actin network in cell motility and chemotaxis. Proc. Natl. Acad. Sci. U.S.A. 102, 7601–7606.

DiMauro, S., 2004. Mitochondrial diseases. Biochim. Biophys. Acta 1658, 80–88.

Eichinger, L., Pachebat, J.A., Glockner, G., Rajandream, M.A., Sucgang, R., Berriman, M., Song, J., Olsen, R., Szafranski, K., Xu, Q., Tunggal, B., Kummerfeld, S., Madera, M., Konfortov, B.A., Rivero, F., Bankier, A.T., Lehmann, R., Hamlin, N., Davies, R., Gaudet, P., Fey, P., Pilcher, K., Chen, G., Saunders, D., Sodergren, E., Davis, P., Kerhornou, A., Nie, X., Hall, N., Anjard, C., Hemphill, L., Bason, N., Farbrother, P., Desany, B., Just, E., Morio, T., Rost, R., Churcher, C., Cooper, J., Haydock, S., van Driessche, N., Cronin, A., Goodhead, I., Muzny, D., Mourier, T., Pain, A., Lu, M., Harper, D., Lindsay, R., Hauser, H., James, K., Quiles, M., Madan Babu, M., Saito, T., Buchrieser, C., Wardroper, A., Felder, M., Thangavelu, M., Johnson, D., Knights, A., Loulseged, H., Mungall, K., Oliver, K., Price, C., Quail, M.A., Urushihara, H., Hernandez, J., Rabbinowitsch, E., Steffen, D., Sanders, M., Ma, J., Kohara, Y., Sharp, S., Simmonds, M., Spiegler, S., Tivey, A., Sugano, S., White, B., Walker, D., Woodward, J., Winckler, T., Tanaka, Y., Shaulsky, G., Schleicher, M., Weinstock, G., Rosenthal, A., Cox, E.C., Chisholm, R.L., Gibbs, R., Loomis, W.F., Platzer, M., Kay,

Author's personal copy

R.R., Williams, J., Dear, P.H., Noegel, A.A., Barrell, B., Kuspa, A., 2005. The genome of the social amoeba *Dictyostelium discoideum*. Nature 435, 43–57.
Fields, S.D., Arana, Q., Heuser, J., Clarke, M., 2002. Mitochondrial membrane dynamics are altered in cluA⁻ mutants of *Dictyostelium*. J. Muscle Res. Cell Motil. 23, 829–838.
Finn, R.D., Mistry, J., Tate, J., Coggill, P., Heger, A., Pollington, J.E., Gavin, O.L., Gunasekaran, P., Ceric, G., Forslund, K., Holm, L., Sonnhammer, E.L., Eddy, S.R., Bateman, A., 2010. The Pfam protein families database. Nucleic Acids Res. 38, D211–D222.
Fransson, A., Ruusala, A., Aspenström, P., 2003. Atypical Rho GTPases have roles in mitochondrial homeostasis and apoptosis. J. Biol. Chem. 278, 6495–6502.
Fransson, A., Ruusala, A., Aspenström, P., 2006. The atypical Rho GTPases Miro-1 and Miro-2 have essential roles in mitochondrial trafficking. Biochem. Biophys. Res. Commun. 344, 500–510.
Frederick, R.L., McCaffery, J.M., Cunningham, K.W., Okamoto, K., Shaw, J.M., 2004. Yeast Miro GTPase, Gem1p, regulates mitochondrial morphology via a novel pathway. J. Cell Biol. 167, 87–98.
Frederick, R.L., Okamoto, K., Shaw, J.M., 2008. Multiple pathways influence mitochondrial inheritance in budding yeast. Genetics 178, 825–837.
Frederick, R.L., Shaw, J.M., 2007. Moving mitochondria: establishing distribution of an essential organelle. Traffic 8, 1668–1675.
Glater, E.E., Megeath, L.J., Stowers, R.S., Schwarz, T.L., 2006. Axonal transport of mitochondria requires milton to recruit kinesin heavy chain and is light chain independent. J. Cell Biol. 173, 545–557.
Guindon, S., Gascuel, O., 2003. A simple, fast, and accurate algorithm to estimate large phylogenies by maximum likelihood. Syst. Biol. 52, 696–704.
Guo, X., Macleod, G.T., Wellington, A., Hu, F., Panchumarthi, S., Schoenfield, M., Marin, L., Charlton, M.P., Atwood, H.L., Zinsmaier, K.E., 2005. The GTPase dMiro is required for axonal transport of mitochondria to Drosophila synapses. Neuron 47, 379–393.
Hestermann, A., Rehberg, M., Gräf, R., 2002. Centrosomal microtubule plus end tracking proteins and their role in *Dictyostelium* cell dynamics. J. Muscle Res. Cell Motil. 23, 621–630.
Iwai, S., Ishiji, A., Mabuchi, I., Sutoh, K., 2004. A novel actin-bundling kinesin-related protein from *Dictyostelium discoideum*. J. Biol. Chem. 279, 4696–4704.
Kilmartin, J.V., Wright, B., Milstein, C., 1982. Rat monoclonal antitubulin antibodies derived by using a new nonsecreting rat cell line. J. Cell Biol. 93, 576–582.
Kollmar, M., Glockner, G., 2003. Identification and phylogenetic analysis of *Dictyostelium discoideum* kinesin proteins. BMC Genomics 4, 47.
Kotsifas, M., Barth, C., de Lozanne, A., Lay, S.T., Fisher, P.R., 2002. Chaperonin 60 and mitochondrial disease in *Dictyostelium*. J. Muscle Res. Cell Motil. 23, 839–852.
Laporte, C., Kosta, A., Klein, G., Aubry, L., Lam, D., Tresse, E., Luciani, M.F., Golstein, P., 2007. A necrotic cell death model in a protist. Cell Death Differ. 14, 266–274.
Li, Y., Lim, S., Hoffman, D., Aspenström, P., Federoff, H.J., Rempe, D.A., 2009. HUMMR, a hypoxia- and HIF-1alpha-inducible protein, alters mitochondrial distribution and transport. J. Cell Biol. 185, 1065–1081.
Lingnau, A., Chakraborty, T., Niebuhr, K., Domann, E., Wehland, J., 1996. Identification and purification of novel internalin-related proteins in Listeria monocytogenes and Listeria ivanovii. Infect. Immun. 64, 1002–1006.
Liu, X., Hajnoczky, G., 2009. Ca^{2+}-dependent regulation of mitochondrial dynamics by the Miro-Milton complex. Int. J. Biochem. Cell Biol. 41, 1972–1976.
MacAskill, A.F., Rinholm, J.E., Twelvetrees, A.E., Arancibia-Carcamo, I.L., Muir, J., Fransson, A., Aspenstrom, P., Attwell, D., Kittler, J.T., 2009a. Miro1 is a calcium sensor for glutamate receptor-dependent localization of mitochondria at synapses. Neuron 61, 541–555.
MacAskill, A.F., Rinholm, J.E., Twelvetrees, A.E., Arancibia-Carcamo, I.L., Muir, J., Fransson, A., Aspenström, P., Attwell, D., Kittler, J.T., 2009b. Miro1 is a calcium sensor for glutamate receptor-dependent localization of mitochondria at synapses. Neuron 61, 541–555.
McBride, H.M., Neuspiel, M., Wasiak, S., 2006. Mitochondria: more than just a powerhouse. Curr. Biol. 16, R551–R560.
Newell, P.C., Telser, A., Sussmann, M., 1969. Alternative developmental pathways determined by environmental conditions in the cellular slime mold *Dictyostelium discoideum*. J. Bacteriol. 100, 763–768.
Noegel, A.A., Rivero, F., Albrecht, R., Janssen, K.P., Kohler, J., Parent, C.A., Schleicher, M., 1999. Assessing the role of the ASP56/CAP homologue of *Dictyostelium discoideum* and the requirements for subcellular localization. J. Cell Sci. 112, 3195–3203.
Pawlowski, J., Burki, F., 2009. Untangling the phylogeny of amoeboid protists. J. Eukaryot. Microbiol. 56, 16–25.
Pei, J., Grishin, N., 2007. PROMALS: towards accurate multiple sequence alignments of distantly related proteins. Bioinformatics 23, 802–808.
Pendergrass, W., Wolf, N., Poot, M., 2004. Efficacy of MitoTracker Green and CMXrosamine to measure changes in mitochondrial membrane potentials in living cells and tissues. Cytometry A 61, 162–169.
Pollock, N., de Hostos, E.L., Turck, C.W., Vale, R.D., 1999. Reconstitution of membrane transport powered by a novel dimeric kinesin motor of the Unc104/KIF1A family purified from *Dictyostelium*. J. Cell Biol. 147, 493–505.
Reis, K., Fransson, A., Aspenström, P., 2009. The Miro GTPases: at the heart of the mitochondrial transport machinery. FEBS Lett. 583, 1391–1398.
Rivero, F., Albrecht, R., Dislich, H., Bracco, E., Graciotti, L., Bozzaro, S., Noegel, A.A., 1999. RacF1, a novel member of the Rho protein family in *Dictyostelium discoideum*, associates transiently with cell contact areas, macropinosomes and phagosomes. Mol. Biol. Cell 10, 1205–1219.
Rivero, F., Koppel, B., Peracino, B., Bozzaro, S., Siegert, F., Weijer, C.J., Schleicher, M., Albrecht, R., Noegel, A.A., 1996. The role of the cortical cytoskeleton: F-actin crosslinking proteins protect against osmotic stress, ensure cell size, cell shape and motility, and contribute to phagocytosis and development. J. Cell Sci. 109, 2679–2691.
Rivero, F., Maniak, M., 2006. Quantitative and microscopic methods for studying the endocytic pathway. Methods Mol. Biol. 346, 423–438.
Röhlk, C., Rohlfs, M., Leier, S., Schliwa, M., Liu, X., Parsch, J., Woehlke, G., 2008. Properties of the Kinesin-1 motor DdKif3 from *Dictyostelium discoideum*. Eur. J. Cell Biol. 87, 237–249.
Russo, G.J., Louie, K., Wellington, A., Macleod, G.T., Hu, F., Panchumarthi, S., Zinsmaier, K.E., 2009. *Drosophila* Miro is required for both anterograde and retrograde axonal mitochondrial transport. J. Neurosci. 29, 5443–5455.
Saotome, M., Safiulina, D., Szabadkai, G., Das, S., Fransson, A., Aspenström, P., Rizzuto, R., Hajnoczky, G., 2008. Bidirectional Ca^{2+}-dependent control of mitochondrial dynamics by the Miro GTPase. Proc. Natl. Acad. Sci. U.S.A. 105, 20728–20733.
Schiavo, G., Bisson, R., 1989. Oxygen influences the subunit structure of cytochrome c oxidase in the slime mold Dictyostelium discoideum. J. Biol. Chem. 264, 7129–7134.
Simpson, P.A., Spudich, J.A., Parham, P., 1984. Monoclonal antibodies prepared against *Dictyostelium* actin: characterization and interaction with actin. J. Cell Biol. 1, 287–295.
Soding, J., Biegert, A., Lupas, A.N., 2005. The HHpred interactive server for protein homology detection and structure prediction. Nucleic Acids Res. 33, W244–W248.
Stamatakis, A., Hoover, P., Rougemont, J., 2008. A rapid bootstrap algorithm for the RAxML Web servers. Syst. Biol. 57, 758–771.
Torija, P., Vicente, J.J., Rodrigues, T.B., Robles, A., Cerdan, S., Sastre, L., Calvo, R.M., Escalante, R., 2006. Functional genomics in Dictyostelium: MidA, a new conserved protein, is required for mitochondrial function and development. J. Cell Sci. 119, 1154–1164.
Troll, H., Malchow, D., Müller-Taubenberger, A., Humbel, B., Lottspeich, F., Ecke, M., Gerisch, G., Schmid, A., Benz, R., 1992. Purification, functional characterization, and cDNA sequencing of mitochondrial porin from *Dictyostelium discoideum*. J. Biol. Chem. 267, 21072–21079.
van Es, S., Wessels, D., Soll, D.R., Borleis, J., Devreotes, P.N., 2001. Tortoise, a novel mitochondrial protein, is required for directional responses of *Dictyostelium* in chemotactic gradients. J. Cell Biol. 152, 621–632.
Wang, X., Schwarz, T.L., 2009. The mechanism of Ca^{2+}-dependent regulation of kinesin-mediated mitochondrial motility. Cell 136, 163–174.
Wattenberg, B., Lithgow, T., 2001. Targeting of C-terminal (tail)-anchored proteins: understanding how cytoplasmic activities are anchored to intracellular membranes. Traffic 2, 66–71.
Weihofen, A., Thomas, K.J., Ostaszewski, B.L., Cookson, M.R., Selkoe, D.J., 2009. Pink1 forms a multiprotein complex with Miro and Milton, linking Pink1 function to mitochondrial trafficking. Biochemistry 48, 2045–2052.
Westphal, M., Jungbluth, A., Heidecker, M., Muhlbauer, B., Heizer, C., Schwartz, J.M., Marriott, G., Gerisch, G., 1997. Microfilament dynamics during cell movement and chemotaxis monitored using a GFP-actin fusion protein. Curr. Biol. 7, 176–183.
Yamaoka, S., Leaver, C.J., 2008. EMB2473/MIRO1, an Arabidopsis Miro GTPase, is required for embryogenesis and influences mitochondrial morphology in pollen. Plant Cell. 20, 589–601.